

EFFECT OF SINGLE-WALLED CARBON NANOTUBES ON THE ADSORPTION OF BASIC RED 12 DYE BY TRIMELLITIC ANHYDRIDE ISOTHIOCYANATE-CROSSLINKED CHITOSAN HYDROGEL

NOUF F. AL-HARBY,* MAWAHEB S. ALMARSHED* and NADIA A. MOHAMED**

*Department of Chemistry, College of Science, Qassim University,
Buraidah 51452, Saudi Arabia

**Department of Chemistry, Faculty of Science, Cairo University, Giza 12613, Egypt

✉ Corresponding author: N. F. Al-Harby, hrbien@qu.edu.sa

Received January 11, 2023

A chitosan hydrogel crosslinked with the least amount of trimellitic anhydride isothiocyanate (H_1) and filled with 0.6 wt% of single-walled carbon nanotubes (SWCNTs) (H_1 /SWCNTs) was synthesized. Its structure was proven *via* Fourier transform infrared (FTIR) spectroscopy, X-ray diffraction (XRD), scanning electron microscopy (SEM) and transmission electron microscopy (TEM) observations. The adsorption capacity of H_1 /SWCNTs for Basic red 12 (BR 12) dye, at pH 7 and 25 °C, was 14.80 mg g⁻¹ with a percent removal efficiency of 37.66%, which was greater by 1.8 times than that of the parent hydrogel H_1 (8.21 mg g⁻¹ and 20.90%, respectively). Its sorption capacity slightly enhanced with decreasing adsorption solution pH. The optimum adsorption capacity of 15.62 mg g⁻¹ and the % removal efficiency of 39.76% were observed at pH 10 and 25 °C. The adsorption of BR 12 dye onto H_1 /SWCNTs at different temperatures and different dye solution pH values fitted to the pseudo-second order and the intraparticle diffusion kinetic models. The adsorption isotherm for BR 12 dye by H_1 /SWCNTs fitted to the Langmuir isotherm model, indicating the monolayer nature of adsorption. BR 12 dye adsorption onto H_1 /SWCNTs is an exothermic process. Thus, the inclusion of SWCNTs into the matrices of functionalized chitosan hydrogel H_1 improved its features. It is a suitable way to obtain a favorable composite with high-performance adsorbing characteristic for cationic dyes removal.

Keywords: chitosan hydrogel/SWCNTs composite, Basic Red 12 dye, adsorption, kinetics, adsorption isotherms, adsorption thermodynamics

INTRODUCTION

Highly purified water is an essential demand for the physiological activities of the living organisms. Numerous kinds of non-biodegradable commercial dyes are discharged into industrial wastewater, causing water pollution.¹ The removal of these dyes from industrial streams is essential before discharging them into the environment since some of them are carcinogenic, teratogenic, mutagenic and toxic.² The cationic dyes are more toxic than the anionic ones.³ Several traditional physico-chemical techniques have been used for the treatment of industrial wastewater, such as electrocoagulation,⁴ photocatalytic degradation,⁵ flocculation,⁶ reverse osmosis,⁷ membrane filtration,⁸ ion exchange,⁹ biodegradation,¹⁰ oxidation–ozonation¹¹ and chemical precipitation.¹² Despite the fact that these techniques have shown high efficiency, some

issues related to their use include high energy consumption, high costs and toxic by-product production from the chemicals used, in addition to poor performance at low dye concentration.

The most efficient technique used for removing dyes from aqueous medium is the adsorption process, particularly when the adsorbents are cheap, abundant and easily obtainable.¹³⁻¹⁵ In addition, the adsorption process is characterized by high performance, simplicity, ease of operation, high possibility of restoring and reusing the adsorbents, and its use does not result in any harmful by-products.¹⁶⁻¹⁸

Chitosan is one of the most promising biopolymers, possessing some interesting properties, such as water binding capacity, antimicrobial activity, fat binding capacity, biocompatibility and bio-degradability, its

degradation products are non-toxic, non-immunogenic, and non-carcinogenic.^{14,19,20} Chitosan acts as an efficient adsorbent of anionic dyes due to its unique polycationic character,^{21,22} but it is not a good adsorbent for the adsorption of cationic dyestuffs. Chitosan is readily soluble in acidic solutions with degradation, restricting its utilization as adsorbent for removing the dyes from their effluents, which are usually acidic. Thus, controlling the solubility of chitosan in acidic solutions is a desirable property for such application. Therefore, it is essential to develop a stable and durable polymeric material, based on chitosan, controlling both its solubility and its adsorption characteristics. Modification of chitosan *via* substitution,^{23,24} grafting,^{25,26} blending²⁷⁻²⁹ crosslinking³⁰⁻³⁵ and nanocomposite formation^{30,31,36,37} has been investigated to improve its properties, such as lowering of its solubility, inhibiting its degradation rate, and increasing the life span of its products in different media.

Chitosan has been filled with carbon nanotubes (CNTs) to improve its adsorption capability for various dyes. This can be attributed to their nano-sized layered hollow structures, together with a great surface area. CNTs have a strong adsorption interaction with organic aromatic pollutants. This is due to the donating power of π electron of the CNTs and the accepting nature of π electron for the aromatic molecules. The potent surface complexation of ions with functional groups are considered the prime mechanism of adsorption of cationic and anionic dyes onto CNTs.^{38,39}

In our previous studies,^{31,40,41} four chitosan-based hydrogels (H₁-H₄) have been designed and synthesized using different concentrations of trimellitic anhydride isothiocyanate as a crosslinker. The resulted crosslinked chitosan hydrogels possess a variety of bioactive functional groups (thiourea, amide, carboxylic groups), in addition to the residual primary amino groups of chitosan that are not consumed during the crosslinking process. All the prepared hydrogels showed higher chemical stability in acidic media and better antimicrobial activity than those of the parent chitosan.³¹ These amphoteric hydrogels have greater adsorption capacity for both anionic Congo Red dye⁴⁰ and cationic Basic Red 12 (BR 12) dye⁴¹ from their aqueous solutions at a wide range of pH values, compared to chitosan. Since the least crosslinked chitosan hydrogel H₁ showed the lowest adsorption capacity for cationic BR 12 dye relative to the other hydrogels,⁴¹ it became of importance to develop its adsorption capacity for

this dye by incorporating SWCNTs into its matrices. It would be expected that the resulting H₁/SWCNT composites combine the adsorption mechanisms of both the hydrogel H₁ and SWCNTs.⁴¹ For this and for the first time, the present work was directed to study the effect of incorporating SWCNTs into H₁ on its adsorption capacity for BR 12 dye from its aqueous solution at different temperatures and different pH values. The kinetics, isotherms and thermodynamics of the adsorption process were also investigated.

EXPERIMENTAL

Materials

Chitosan (deacetylation degree = 88%, and molecular weight = 2.0×10^5 g mol⁻¹) (Funakoshi Co. Ltd., Japan), glacial acetic acid (99.8%, E. Merck, Darmstadt), trimellitic anhydride chloride (98%, Aldrich), ammonium thiocyanate ($\geq 97.5\%$), polyethylene glycol 400 (99%) and SWCNTs ($\geq 95\%$, Sigma-Aldrich), methylene chloride ($>99.5\%$) and sodium hydroxide pellets (98%, Loba Chemie), sodium carbonate (99-100%, Techno Pharmchem), methanol ($\geq 99.9\%$, HPLC grade, Fisher Chemical), hydrochloric acid (37%, PanReac. AppliChem-ITW Reagent) and BR 12 dye (99% Hoechst, Germany) were used in this study as received. Figure 1 presents the chemical structure of the BR 12 dye.

Synthesis of trimellitic anhydride isothiocyanate-cross linked chitosan hydrogel (H₁)

Crosslinked chitosan hydrogel (H₁) was prepared according to the method described in our previous work.³¹ Briefly, solid trimellitic anhydride chloride (0.53 g, 2.5 mmol) was added as one portion to 40 mL of dichloromethane solution containing ammonium thiocyanate (0.19 g, 2.5 mmol). To this reaction mixture, 1 mL of polyethylene glycol-400 was added as a phase transfer catalyst. The resulting reaction mixture was stirred at room temperature for 2 h and then was filtered to remove the ammonium chloride formed as a white precipitate during the reaction. The filtrate (trimellitic anhydride isothiocyanate) (Scheme 1A) was added to chitosan (6.44 g, 40 mmol) that was dissolved in 400 mL of aqueous acetic acid solution (1% v/v). The reaction mixture was well stirred at 60 °C for 2 h, and then at room temperature overnight to produce H₁ (Scheme 1B).

Fabrication of H₁

The formed crosslinked chitosan hydrogel, H₁, was fabricated to particles of similar sizes by following the process described in our previous work.⁴¹ Briefly, it was dropped from a burette equipped with various micropipette tips into an aqueous sodium carbonate solution as a neutralizing medium for acetic acid. The produced droplets of the hydrogel that appeared as spherical particles in the solution were gently stirred for 24 h until

reaching pH 7, filtered, washed repeatedly with deionized water, soaked in methanol for another 24 h,

filtered again, and finally dried at 60 °C to constant weight.

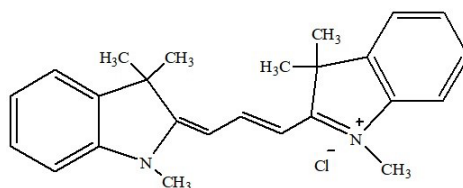
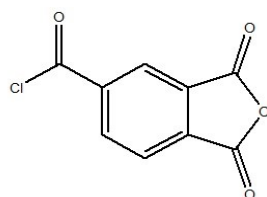
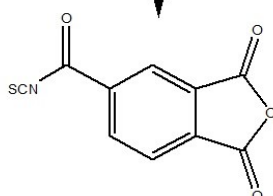


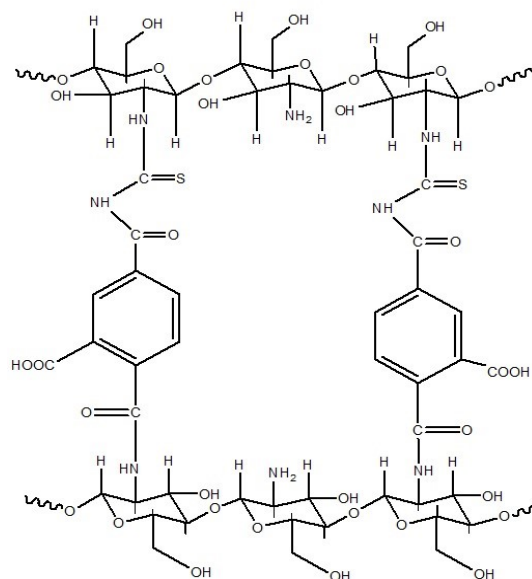
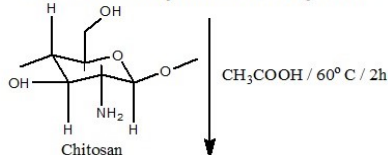
Figure 1: Chemical structure of BR 12 dye



(A) Trimellitic anhydride chloride



(B) Trimellitic anhydride isothiocyanate



Scheme 1: Synthesis of H₁

The particle diameter was governed by the different micro-pipette tips used. These particles were also sieved

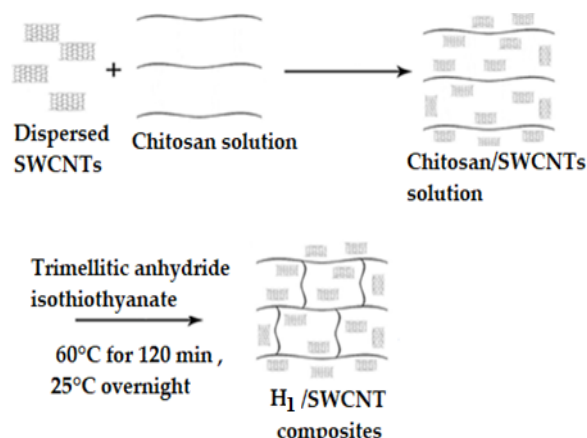
using a suitable mesh to obtain particles having mostly equal size. Thus, four different diameters of the

hydrogel particles were obtained (0.4 mm, 0.8 mm, 1.5 mm and 3 mm), as measured using an electronic micro Vernier caliper. The adsorption capacity (at pH 7 and 25 °C) of the hydrogel particles of various sizes (0.4 mm, 0.8 mm, 1.5 mm and 3 mm) was 14.8, 12.7, 10.8 and 8.6 mg g⁻¹, respectively. This indicated that the greater adsorption capacity was achieved onto hydrogel of 0.4 mm particle size than those of larger sizes (0.8 mm, 1.5 mm and 3 mm). This is ascribed to the larger surface area of the particles of smaller size (0.4 mm). For this reason, the present work has been confined to the study of the kinetics, isotherms, thermodynamics and optimization of the adsorption process of the hydrogel of 0.4 mm particle size to remove the cationic BR 12 dye from its aqueous solution for industrial wastewater treatment.

Synthesis of H₁/SWCNT composites

Four precalculated weight percent of the SWCNTs were separately sonicated in 15 mL of aqueous acetic

acid solution (1% v/v) at 25 °C for 20 min to reach a good dispersion of SWCNTs. Each dispersed SWCNTs was gradually mixed with chitosan (6.44 g, 40 mmol) dissolved in 400 mL of aqueous acetic acid solution (1% v/v) and agitated using a mechanical stirrer at 25 °C for 90 min to realize high dispersion of SWCNTs in the matrices of chitosan. To these mixtures, the same amount of trimellitic anhydride isothiocyanate crosslinker (2.5 mmol) (Scheme 1A), which was utilized to prepare H₁,³¹ was added with continuous mechanical stirring at 60 °C for 120 min and then at 25 °C overnight (Scheme 2). The weight percent of the SWCNTs based on the weight of H₁ was 0.2%, 0.4%, 0.6% and 0.8%, to obtain four nanocomposites, which were fabricated into particles by following the method described above H₁. It was expected that the π -bonds of the sidewalls of the SWCNTs would ionically interact with the functional groups of the crosslinked chitosan hydrogel H₁, leading to the formation of its composites.^{30,31,36}



Scheme 2: Schematic illustration of H₁/SWCNT composites formation

Characterization

FTIR spectroscopy

A Tescan Shimadzu FTIR spectrophotometer (Model 8000, Japan) was used for recording the FTIR spectra of H₁ and H₁/SWCNTs composites for identifying their structures.

X-ray diffractometry

Brucker's D-8 advanced wide-angle X-ray diffractometer was utilized to identify the interior structure of SWCNTs, H₁ and H₁/SWCNTs composites.

Scanning electron microscopy

A scanning electron microscope (SEM) (Jeol-JSM-6060LV) was used for observing the surface topography of H₁ and H₁/SWCNTs composites.

Transmission electron microscopy

A JEM-1400 transmission electron microscope was utilized for identification of the morphological structure of H₁/SWCNTs composites.

UV-visible spectroscopy

A UV-1650 PC Shimadzu spectrophotometer was used to determine the dye concentration *via* measuring the absorbance of its solution at $\lambda_{max} = 485$ nm.

Point of zero-charge (pHpzc)

The pHpzc was determined by soaking the H₁/SWCNTs composite (0.1 g) for 24 h in 10 mL of aqueous NaCl solution (0.1 M), after adjusting its pH in the range from 3 to 12. The pH was adjusted using solutions of 0.1 N HCl and 0.1 N NaOH. Then, the pH of the solution was measured by a pH meter. The pHpzc value was obtained by plotting the graph of initial pH against Δ pH (final pH – initial pH).^{42,43}

Adsorption studies

The adsorbent (50 mg) and BR 12 dye solution (50 mL, 1×10^{-4} mol/L) were mixed into a glass conical flask with shaking at a speed of 80 rpm and at a predetermined temperature in a water bath till reaching equilibrium. The adsorption process was carried out in

the temperature range of 25-55 °C, and at various dye solution pH (4 to 10). Sodium hydroxide solution or hydrochloric acid solution was used to modify the pH of the dye solution.

The adsorption capacity of the adsorbent for the dye at equilibrium time (q_e (mg g⁻¹)) and at time t (q_t (mg g⁻¹)) was quantified by the weight balance relationships (Eqs. 1 and 2, respectively):

$$q_e = \frac{(C_o - C_e) \times V}{W} \quad (1)$$

$$q_t = \frac{(C_o - C_t) \times V}{W} \quad (2)$$

where C_o is the initial concentration of dye, C_e is the dye concentration at equilibrium time and C_t is the dye concentration at time t (mg L⁻¹), V (L) is the dye solution volume and W (g) is the weight of adsorbent.^{44,45}

The removal efficiency percent of the dye in the equilibrium state was determined by Equation 3:⁴⁶

$$\% \text{ Removal efficiency} = \frac{C_o - C_e}{C_o} \times 100 \quad (3)$$

where C_o and C_e are the initial dye concentration and the dye concentration at equilibrium time (mg L⁻¹), respectively.

Adsorption kinetic studies

To explore the mechanism of adsorption for a dye onto an adsorbent, the two kinetic models of the pseudo-first order (Eq. 4) and the pseudo-second order (Eq. 5) are usually applied:

$$\frac{dq_t}{dt} = k_1 (q_e - q_t) \quad (4)$$

$$\frac{dq_t}{dt} = k_2 (q_e - q_t)^2 \quad (5)$$

where q_e and q_t are the quantities of the dyes adsorbed onto the adsorbent at equilibrium time and at different time intervals (mg g⁻¹), respectively, and k_1 (min⁻¹) and k_2 (g mg⁻¹min⁻¹) are the rate constants of the pseudo-first order and the pseudo-second order kinetic models, respectively.⁴⁴

The linear equations for the pseudo-first order and pseudo-second order kinetic models are given in Equations 6 and 7, respectively:^{21,46}

$$\log(q_e - q_t) = \log(q_e) - \frac{k_1 t}{2.303} \quad (6)$$

$$\frac{t}{q_t} = \frac{1}{k_2 q_e^2} + \frac{t}{q_e} \quad (7)$$

Adsorption isotherm studies

The adsorbent (10 mg) was introduced into tubes containing 10 mL of BR 12 dye solution of different concentrations (1×10^{-5} , 2×10^{-5} , 3×10^{-5} , 4×10^{-5} , 5×10^{-5} , 6×10^{-5} , 7×10^{-5} , 8×10^{-5} , 9×10^{-5} and 1×10^{-4} mol L⁻¹) at pH

7 and agitated at a temperature of 55 °C till equilibrium time.

The Langmuir, Freundlich, Temkin and Dubinin–Radushkevich (D–R) isotherm models were used to fit the experimental data. The Langmuir isotherm is presented by Equation 8:

$$\frac{C_e}{q_e} = \frac{1}{q_{\max} K_L} + \frac{C_e}{q_{\max}} \quad (8)$$

where q_e , C_e , q_{\max} , K_L are the amount of dye adsorbed at equilibrium (mg g⁻¹), the dye concentration in solution at equilibrium (mg L⁻¹), the monolayer sorption capacity (mg g⁻¹) and the Langmuir constant (L mg⁻¹), respectively.

The affinity between the adsorbate and the adsorbent can be obtained from the Langmuir parameter with the help of the dimensionless separation factor (R_L), which can be presented by Equation 9:

$$R_L = \frac{1}{(1 + K_L C_o)} \quad (9)$$

The Freundlich isotherm is presented using Equations 10 and 11:

$$q_e = K_F C_e^{1/n} \quad (10)$$

$$\ln q_e = \ln K_F + \frac{1}{n} \ln C_e \quad (11)$$

where K_F is the equilibrium adsorption coefficient (mg g⁻¹) (L mg⁻¹), and $1/n$ is the empirical constant. In fact, the n value depicts the favorability of the adsorption process and K_F is the adsorption capacity and intensity of the adsorbate.^{21,46,47}

The Temkin model assumes the decrease in the heat uptake for dye molecules with surface saturation under the effect of continuous interaction between the studied adsorbent and dye molecules. The Temkin model can be expressed by Equation 12:

$$q_e = B \ln K_T + B \ln C_e \quad (12)$$

where B is the Temkin constant that is controlled by the adjusted uptake in temperature (J mol⁻¹), K_T is the binding constant of the Temkin isotherm (L g⁻¹), q_e is the amount of dye adsorbed at equilibrium (mg g⁻¹), and C_e is the dye equilibrium concentration at a constant temperature (mg L⁻¹). By plotting q_e against $\ln C_e$, the constants B and K_T can be obtained from the slope and the intercept, respectively.

The Dubinin–Radushkevich (D–R) model is used for estimating the free energy of adsorption and the characteristic porosity. This model can successfully help in determining the type of the adsorption process whether it is chemisorption or physisorption. The D–R isotherm model doesn't assume that the surface is homogenous; so, it is more general than Langmuir isotherm. The D–R isotherm is given by Equation 13:

$$\ln q_e = \ln (X_m) - \beta \epsilon^2 \quad (13)$$

where q_e is the amount of dye adsorbed at equilibrium (mg g⁻¹), X_m is the monolayer saturation capacity (mg g⁻¹), β is the activity coefficient that is related to

adsorption mean free energy ($\text{mol}^2 \text{ j}^{-2}$), and ε is the Polanyi potential, which is determined by Equation 14:

$$\varepsilon = RT \ln \left(1 + \frac{1}{C_e} \right) \quad (14)$$

where R is the universal gas constant ($8.314 \text{ J mol}^{-1} \text{ K}^{-1}$) and T is the absolute temperature (K).

By plotting $\ln q_e$ versus ε^2 using Equation 13, a straight line is obtained with a slope and intercept of β and $\ln X_m$, respectively. The mean free energy of adsorption, E , (kJ mol^{-1}) can be determined by Equation 15:

$$E = \frac{1}{(2\beta)^{0.5}} \quad (15)$$

This means that the free energy can determine the type of adsorption; if $8 < E < 16 \text{ kJ mol}^{-1}$ the process is chemisorption, while if it is less than 8 kJ mol^{-1} , the process is physisorption.²¹

RESULTS AND DISCUSSION

Preliminary investigations of the adsorption capacity (at pH 7 and $25 \text{ }^\circ\text{C}$) of the four prepared H_1/SWCNT composites, containing 0.2, 0.4, 0.6 and 0.8 wt% of SWCNTs, revealed that the two nanocomposites that contained 0.2 and 0.4 wt% of SWCNTs did not show any improvement in the adsorption capacity relative to H_1 . This may be attributed to their lower content of SWCNTs. The incorporation of 0.6 wt% of SWCNTs into H_1 enhanced the adsorption capacity of the produced nanocomposite by 1.8 times, compared to that obtained by the parent hydrogel H_1 . No further boosting in the adsorption capacity of the nanocomposites was observed when the inserted SWCNTs increased from 0.6 to 0.8 wt%. Thus, 0.6 wt% of SWCNTs was sufficient to reinforce the adsorption capacity of the produced nanocomposite. For this reason, the present work has been confined to studying the adsorption capacity of the nanocomposite containing 0.6 wt% of SWCNTs (denoted as H_1/SWCNTs) for BR 12 dye from its aqueous solution.

Transmission electron microscopy (TEM) of H_1/SWCNTs composite

The insertion of SWCNTs into H_1 was confirmed using TEM observation. The presence of homogeneously dispersed SWCNTs was demonstrated in Figure 2 (a). This can be attributed to the fact that the SWCNTs interacted ionically with the functional groups of H_1 .

X-ray diffraction analysis of H_1/SWCNTs composite

The orderly structure and crystalline pattern of SWCNTs are represented by two specific peaks at diffraction angles of 26.8° (intensive) and 46.5°

(very weak),⁴¹ whilst H_1 is completely amorphous (Fig. 2 (b)). The diffraction pattern of H_1/SWCNTs included both peaks of SWCNTs, suggesting the incorporation of SWCNTs into the matrices of H_1 . This indicates the spreading of SWCNTs into H_1 matrices, padding their interior spaces, leading to the formation of H_1/SWCNTs .

FTIR spectroscopy of H_1 and H_1/SWCNTs composite

FTIR spectra of H_1 and H_1/SWCNTs (Fig. 2 (c)) confirmed the interaction that occurred between the functional groups of H_1 and the π -bonds of the sidewall of the SWCNTs either *via* shifting of some absorption bands to lower frequencies or by the appearance of some new absorption bands. The stretching vibration peak that related to NH groups for H_1 at 3436 cm^{-1} was shifted to a lower wavenumber at 3418 cm^{-1} in H_1/MWCNTs , denoting the participation of these groups in the interaction with SWCNTs. This supports previously published data.⁴⁸ A new absorption peak at 2850 cm^{-1} in H_1/SWCNTs appeared, suggesting the efficient incorporation of SWCNTs inside the matrix of the H_1 . There is a little shift in the absorption peak of the COOH groups of H_1 at 1728 cm^{-1} to a lower frequency at 1720 cm^{-1} in the H_1/SWCNTs , indicating that these groups interacted with SWCNTs. The absorption peak at 1655 cm^{-1} in H_1 , attributable to the overlapped CO (amide), NH (secondary amide), and C=C (aromatic), was shifted to 1635 cm^{-1} in H_1/SWCNTs , referring to its overlapping with the vibrational frequency of the C=C bonds of the inserted SWCNTs. The absorption peaks related to N-C-S groups in H_1 at 1423 and 590 cm^{-1} have shifted to 1416 and 580 cm^{-1} in H_1/SWCNTs . Further, the absorption peak (intensive and broad), attributed to the overlapped C=S with C-O groups, has shifted from 1065 cm^{-1} to 1055 cm^{-1} in H_1/SWCNTs . These differences in the spectra confirm the successful preparation of H_1/SWCNTs .

Scanning electron microscopy (SEM) of H_1/SWCNTs composite

After SWCNTs have been incorporated into H_1 , the surface topography of the formed nanocomposite was significantly changed – its surface became very rough (Fig. 2 (e)), in comparison with the surface topography of its parent H_1 (Fig. 2 (d)). The SWCNTs were regularly distributed on the H_1 composite surface in a distinctive mode.

Point of zero-charge (pH_{pzc})

The pH of the zero-charge point is defined as the pH at which the surface net charge becomes equal to zero under certain conditions of temperature and aqueous solution composition. This does not imply that the surface has no charge at pH_{pzc}, but rather there are equal amounts of positive and negative charges. The magnitude of the surface charge depends on the abundance and types of functional groups, and on the pH of the solution. The pH_{pzc} plays an important role in surface characterization, as it dictates how easily an adsorbent can bind potentially harmful ions. This is due to the fact that the adsorbent surface

bears a net negative charge at pH > pH_{pzc}, making the adsorption of cationic species more favorable. Conversely, for pH < pH_{pzc} value, the adsorbent surface bears a net positive charge $-\text{NH}_3^+$ capable of repelling cations. The pH_{pzc} value for the H₁/SWCNTs composite obtained using the salt addition method was found to be 7 (Fig. 3). The surface of the H₁/SWCNTs composite becomes more anionic by the increase in the pH value. This is attributed to the deprotonation of the carboxylic groups of the crosslinking linkages into the carboxylate anions ($-\text{COO}^-$).^{42,43}

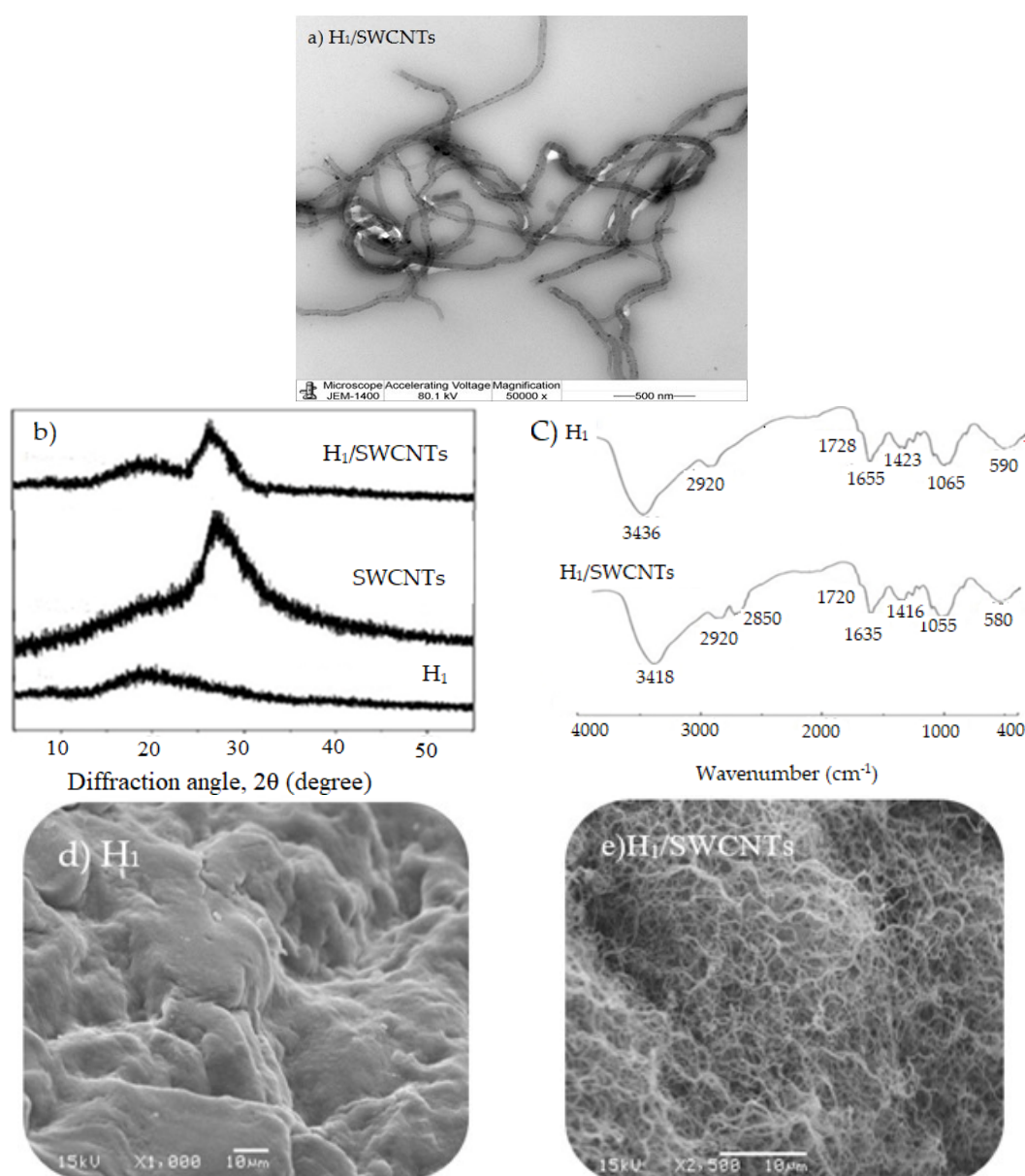
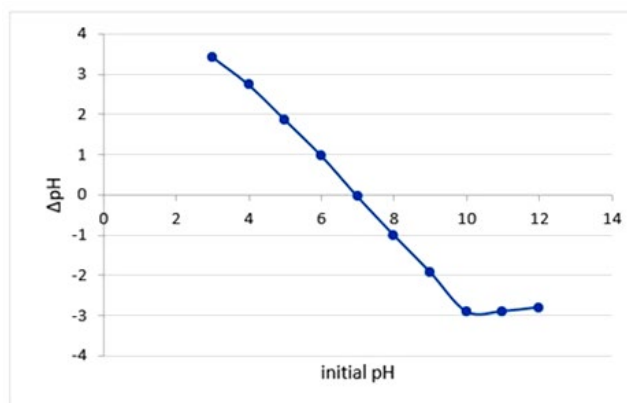


Figure 2: TEM image (a), X-ray diffraction patterns (b), FTIR spectra (c), and SEM images (d) and (e) for H₁ and H₁/SWCNTs composite

Figure 3: pH_{pzc} plot for H₁/SWCNTs composite

Removal of BR 12 dye by H₁/SWCNTs composite

Effect of temperature

Figure 4 (a) shows the results obtained in terms of the adsorption capacity of H₁/SWCNTs for BR 12 dye as a function of time at 25, 35, 45 and 55 °C. The optimum adsorption capacity of H₁/SWCNTs was obtained at 25 °C. No further improvement in the adsorption capacity was observed at temperatures above 25 °C. The adsorption capacity (q_e , Eq. 1) of H₁/SWCNTs was 14.80, 13.15, 12.54 and 12.33 (mg g⁻¹) at 25, 35, 45 and 55 °C, respectively (Fig. 4 (a)). The percent removal efficiency (Eq. 3) of the BR 12 dye was 37.66, 33.47, 31.90 and 31.38% at 25, 35, 45 and 55 °C, respectively. Thus, the adsorption process of BR 12 dye on H₁/SWCNTs was exothermic and the adsorption was impeded by increasing temperature. This may be explained by to the desorption process resulted from the breakdown of adsorption forces that were liable for the adsorption of dye molecules on the adsorbent surface, which might be due to damaging of active sites and the weakening of adsorptive forces between active binding sites of the adsorbent and the adsorbate species.^{49,50} This result is in good agreement with the adsorption of Methylene Blue and Orange II dyes on carbon nanomaterials from aqueous solutions.⁵¹ Interestingly, at 25 °C the adsorption capacity (q_e) and consequently % removal efficiency of H₁/SWCNTs are greater by 1.8 times than those of H₁ (8.21 mg g⁻¹ and 20.90%, respectively) reported in our previous work.⁴¹ This may be attributed to the incorporated SWCNTs into the matrix of H₁.

In general, the adsorption of organic materials onto carbon nanoparticles may originate through

the formation of covalent bonds, hydrogen bonds, electrostatic interactions, $\pi - \pi$ bonds, and hydrophobic interactions.⁵² The high π electrons density of sp² carbons of the sidewalls of CNTs causes their high hydrophobicity. Thus, the hydrophobic interaction may be responsible for the adsorption of dyes onto the sidewalls of CNTs.⁵³ The bulk π system of CNTs and the C=C or benzene rings of the dye molecules may interact through $\pi - \pi$ bonding.^{54,55} The interaction of BR 12 dye with the SWCNTs is presented in Scheme 3.

Effect of dye solution pH

Figure 4 (b) shows the effect of the dye solution pH (4, 7 and 10) on the adsorption kinetics of BR 12 dye onto H₁/SWCNTs at the temperature of 25 °C. The optimum adsorption capacity (q_e , Eq. 1) (15.62 mg g⁻¹) and the % removal efficiency (Eq. 3) (39.76%) of H₁/SWCNTs for BR 12 dye at pH 10 were greater than those obtained at pH 7 (14.80 mg g⁻¹ and 37.66%, respectively). Meanwhile, no adsorption was observed at pH 4. Interestingly, at pH 7, the adsorption capacity (q_e) and the % removal efficiency of H₁/SWCNTs are higher by 1.8 times than those of H₁ reported in our previous work.⁴¹ This is supported by the study on the adsorption of Methylene Blue dye on carbon nanotubes from aqueous solutions.⁵¹ At low pH (pH 4), the positively charged adsorbent surface (polycationic hydrogel) is considerably repulsed with the cationic dye, resulting in hindering the adsorption. On the other hand, at high pH (pH 10), the positively charged cationic dye is attracted effectively to the negatively charged adsorbent surface (polyanionic hydrogel).⁵⁶

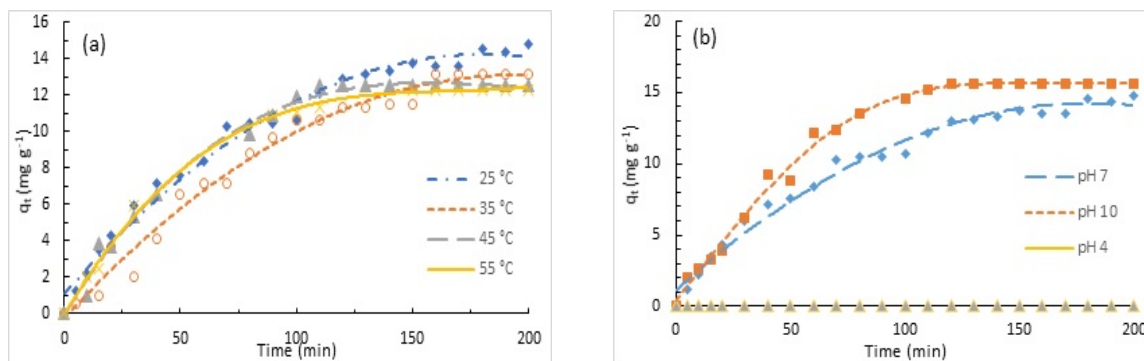
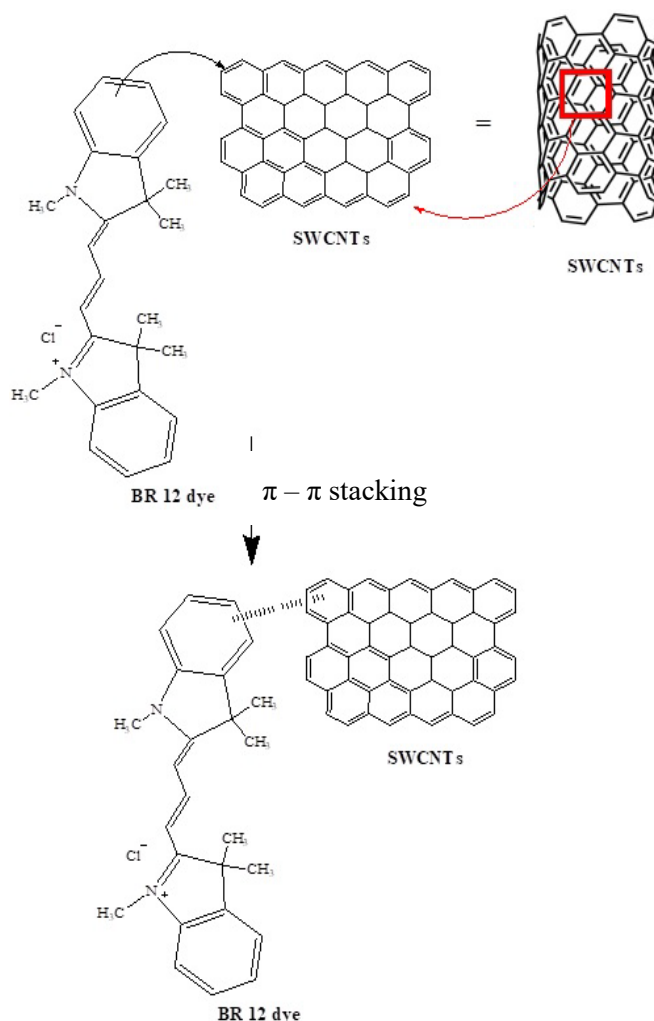


Figure 4: Adsorption of BR 12 dye onto H₁/SWCNTs composite (adsorbent dose = 50 mg, initial dye concentration 1×10^{-4} mol L⁻¹ and volume of dye solution = 50 mL): (a) Effect of temperature at pH 7, (b) Effect of dye solution pH at 25 °C



Scheme 3: Schematic illustration of the interaction mechanism of BR 12 dye with SWCNTs

Adsorption kinetics

The results for the adsorption kinetics of BR 12 dye onto H₁/SWCNTs at dye concentration of 1×10^{-4} mol L⁻¹, adsorbent dose of 50 mg, at different temperatures (25, 35, 45 and 55 °C) and at different solution pH (4, 7 and 10) are shown in Figures 5 and 6, respectively. The different kinetic

parameters of the pseudo-first order and pseudo-second order models for BR 12 dye adsorption onto H₁/SWCNTs at different temperatures and at different pH values were summarized in Table 1.

To investigate the kinetic mechanism that affects the adsorption process, the pseudo-first order (Eq. 6) and the pseudo-second order (Eq. 7)

models were applied to interpret the experimental results. The correlation coefficient (R^2) values for the pseudo-second order kinetic model were 0.973, 0.980, 0.920 and 0.987 at 25, 35, 45 and 55 °C, respectively, which are higher than the corresponding R^2 for the pseudo-first order kinetic model (0.917, 0.786, 0.869 and 0.924) (Table 1). Moreover, Figure 5 demonstrates that the pseudo-second order kinetic model describes better the adsorption process than the pseudo-first order kinetic model for H_1 /SWCNTs at different temperatures. Also, the correlation coefficient (R^2) values for the pseudo-second order kinetic model were 0.973 and 0.961 at pH 7 and 10, respectively, which are greater than their corresponding R^2 of the pseudo-first order kinetic model (0.917 and 0.829) (Table 1). In addition, the values of q_e (cal.)

determined from the pseudo-second order model are close to the q_e (exp.) values. Therefore, the adsorption kinetics of the BR 12 dye on H_1 /SWCNTs follows the pseudo-second order kinetics, suggesting a chemisorption process. Figure 6 also illustrates that the pseudo-second order kinetic model describes better the adsorption process than the pseudo-first order kinetic model for H_1 /SWCNTs at different pH. This supports the findings of a previous study on the removal of Methylene Blue from aqueous solution with magnetite loaded multi-wall carbon nanotube⁵⁷ and those on the adsorption of AB113 dye on C- Fe_2O_3 .⁵⁸ Further, from Table 1, the adsorption rate constant k_2 and the equilibrium adsorption capacity (q_e) of H_1 /SWCNTs for BR 12 dye increased with increasing pH value.

Table 1
Kinetic model constants and correlation coefficients for adsorption of BR 12 dye onto H_1 /SWCNTs composite at different temperatures and at different pH values

Kinetic model	Parameter	Temperature			
		25 °C	35 °C	45 °C	55 °C
	q_e (mg g ⁻¹)	14.80	13.15	12.54	12.33
Pseudo-first order	$k_1 \times 10^{-4}$ (min ⁻¹)	122.06	292.48	204.97	191.15
	R^2	0.917	0.786	0.869	0.924
	$q_{cal.}$	20.83	16.39	15.15	14.29
Pseudo-second order	$k_2 \times 10^{-4}$ (g mg ⁻¹ min ⁻¹)	5.257	6.791	7.724	9.396
	R^2	0.973	0.980	0.920	0.987

Kinetic model	Parameter	pH		
		4	7	10
	q_e (mg g ⁻¹)	0.00	14.80	15.62
Pseudo-first order	$k_1 \times 10^{-4}$ (min ⁻¹)	0.00	122.06	216.48
	R^2	0.00	0.917	0.829
	$q_{cal.}$	0.00	20.83	22.22
Pseudo-second order	$k_2 \times 10^{-4}$ (g mg ⁻¹ min ⁻¹)	0.00	5.257	6.648
	R^2	0.00	0.973	0.961

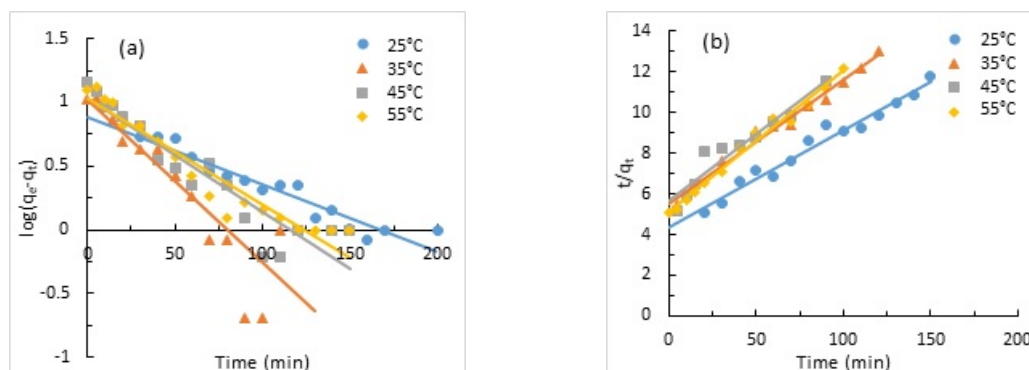


Figure 5: Pseudo-first order (a) and pseudo-second order (b) for BR 12 dye adsorption onto H_1 /SWCNTs composite at different temperatures

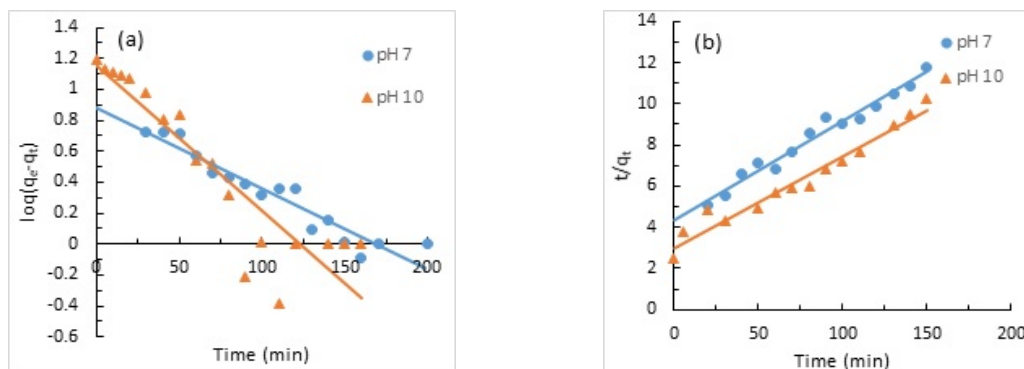


Figure 6: Pseudo-first order (a) and pseudo-second order (b) for BR 12 dye adsorption onto H₁/SWCNTs composite at different pH values

Adsorption isotherms

Adsorption isotherms investigation was performed to examine the adsorption capacities and to elucidate the adsorption mechanism of BR 12 dye onto the H₁/SWCNTs surface at the adsorption equilibrium. The data obtained for the adsorption of BR 12 dye onto H₁/SWCNTs under the best conditions (10 mg of composite, 10 mL of neutral dye solution, and 25 °C) were analyzed by Langmuir (Eq. 8), Freundlich (Eq. 11), Temkin (Eq. 12) and D-R (Eq. 13). The Langmuir isotherm model is based on the assumption that there is homogeneity along the surface of the adsorbent since adsorption binding sites had equal affinity and energy, each adsorbent site is occupied by only one dye molecule and no further adsorption occurs at these sites. Thus, the adsorption nature is a monolayer process. The Freundlich isotherm model is used to describe heterogeneous adsorption systems, assuming that the reactions take place in several sorption sites and the adsorption is a multilayer process.^{46,59,60}

The linear form of Langmuir, Freundlich, Temkin and D-R isotherm equations, for the adsorption of BR 12 dye onto H₁/SWCNTs, is shown in Figure 7. The values of all the adsorption isotherm parameters, with the values of correlation coefficients (R^2), are displayed in Table 2. It is apparent that the Langmuir isotherm fitted better to the experimental data, compared to the other models, with the highest correlation coefficient value R^2 (0.999), compared to that of the Freundlich isotherm model (0.936), Temkin isotherm model (0.975) and D-R isotherm model (0.965). This is consistent with the results of another study on the removal of Methylene Blue from aqueous solution with magnetite loaded

multi-wall carbon nanotube.⁵⁷ For the Freundlich model, the value of the empirical constant n^{-1} was less than 1.0, indicating favorable adsorption of the dye onto the H₁/SWCNTs. This is in agreement with other previously reported results.^{61,57} The adsorption processes were defined based on the separation factor (R_L) value. It is irreversible, linear, unfavorable or favorable when R_L value is equal zero, 1, more than 1 or $0 < R_L < 1$, respectively.⁴³ In this study, the value of R_L is < 1 , indicating a favorable adsorption process of BR 12 dye onto H₁/SWCNTs. This is in agreement with previously reported findings.⁵⁷

Comparison between the efficiency of H₁/SWCNTs and other adsorbents for BR 12 dye removal

To evaluate the efficacy of the H₁/SWCNTs composite, the adsorbent under study, its maximum adsorption capacity for BR 12 dye has been compared with those of other previously reported adsorbents. The H₁/SWCNTs adsorbent was more efficient in adsorbing BR 12 dye than some of the reported adsorbents,^{41,62} but less efficient than others,^{41,62,63} as listed in Table 3. This supports the promising potential of the designed H₁/SWCNTs composite in applications for the removal of BR 12 dye from its aqueous solution.

Thus, in the present study, environmentally friendly chitosan has been modified in order to obtain an increase in the assorted anionic sites, in addition to incorporating SWCNTs into its matrix for effective adsorption of cationic BR 12 dye. The findings suggest the possibility of applying the H₁/SWCNTs composite for removal of BR 12 dye from its aqueous solutions.

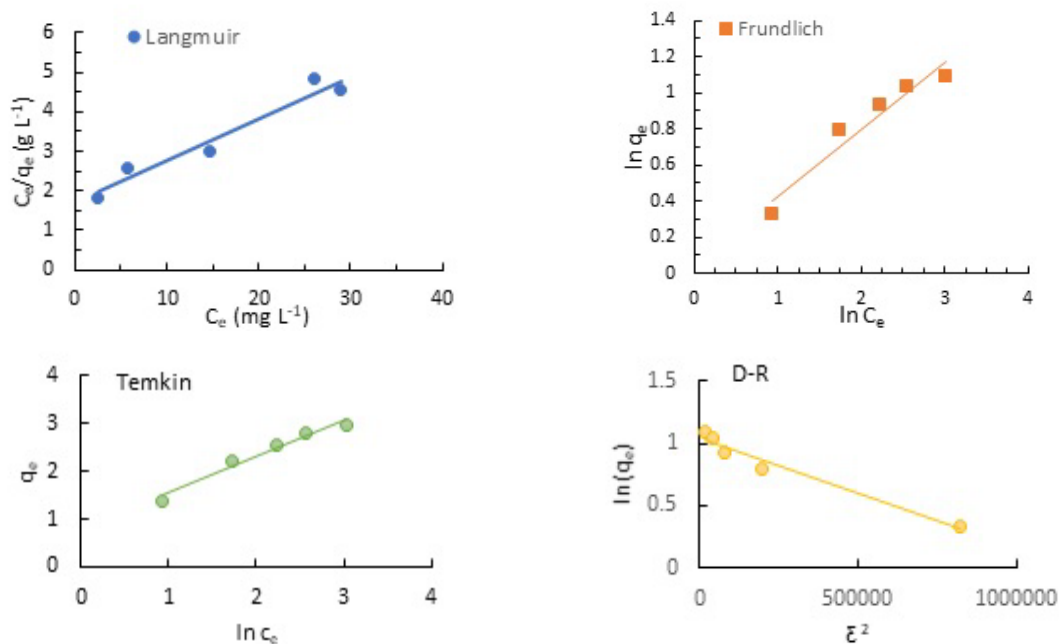


Figure 7: Linear Langmuir, Freundlich, Temkin and D-R isotherm models for the adsorption of BR 12 dye onto H₁/SWCNTs composite

Table 2
Langmuir, Freundlich, Temkin and D-R isotherm constants for adsorption of BR 12 dye onto H₁/SWCNTs composite at 25 °C

Isotherm model	Parameters	Value
Langmuir	R ²	0.999
	K _L (L mg ⁻¹)	0.273
	R _L	0.959-0.996
Freundlich	R ²	0.936
	K _f (L mg ⁻¹)	1.063
	1/n	0.369
Temkin	R ²	0.975
	K _T (L mg ⁻¹)	2.653
	B (J mol ⁻¹)	0.776
D-R	R ²	0.965
	X _{max} (mg g ⁻¹)	2.831
	β (mol ² J ⁻²)	9 x 10 ⁻⁷
	E (kJ mol ⁻¹)	745.356

Table 3
Comparison between the efficiency of H₁/SWCNTs and other adsorbents for BR 12 dye removal

Adsorbents	Removal efficiency (%)	Adsorption capacity (mg/L)	pH	Dye conc. (mg/L)	Temperature (°C)	Refs.
Graphene	5	4	7	80.0	25	62
Graphene oxide	50	40	7	80.0	25	62
Animal bone meal	48.6	29.16	7	60.0	25	63
H1	20.90	8.21	7	39.3	25	41
H2	47.09	18.51	7	39.3	25	41
H3	62.28	24.48	7	39.3	25	41
H1/SWCNTs	39.76	15.63	7	39.3	25	This study

CONCLUSION

The combination between the polyanionic character of trimellitic anhydride isothiocyanate-crosslinked chitosan hydrogel (H_1), which resulted from the presence of the carboxylic groups, and 0.6 wt% SWCNTs enhanced the adsorption capacity of the resulting H_1 /SWCNTs composite for removing cationic BR 12 dye from its aqueous solution. The adsorption capacity of H_1 /SWCNTs was not influenced by the adsorption temperature. Thus, the adsorption capacity of the composite at 25 °C and at pH 7 was 14.80 mg g⁻¹, with a percent removal efficiency of 37.66%, – higher by 1.8 times than the corresponding values obtained for the parent hydrogel H_1 (8.21 mg g⁻¹ and 20.90%, respectively). Also, its sorption capacity slightly enhanced with decreasing adsorption solution pH. The optimum adsorption capacity of 15.62 mg g⁻¹ and the % removal efficiency of 39.76% were observed at pH 10 and 25 °C. The adsorption isotherm data were described well by the Langmuir model, indicating that the BR 12 dye has been chemically adsorbed onto H_1 /SWCNTs. Additionally, the chemical adsorption nature has been evidenced by the fact that the experimental data were fitted well by the pseudo-second order kinetic model. Adsorption thermodynamic results suggested that the adsorption process is exothermic and spontaneous in nature. Accordingly, H_1 /SWCNTs could be applied as an efficient adsorbent for removing of BR 12 dye from its aqueous solution for industrial wastewater treatment.

REFERENCES

- B. Lellis, C. Z. Fávoro-Polonio, J. A. Pamphile and J. C. Polonio, *Biotechnol. Res. Innov.*, **3**, 275 (2019), <https://doi.org/10.1016/j.biori.2019.09.001>
- Z. M. Şenol, N. Gürsoy, S. Şimşek, A. Özer and N. Karakuş, *Int. J. Biol. Macromol.*, **148**, 635 (2020), <https://doi.org/10.1016/j.ijbiomac.2020.01.166>
- T. Madrakian, A. Afkhami, M. Ahmadi and H. Bagheri, *J. Hazard. Mater.*, **196**, 109 (2011), <https://doi.org/10.1016/j.jhazmat.2011.08.078>
- D. Balarak, F. Ganji, S. S. Choi, S. M. Lee and M. J. Shim, *Appl. Chem. Eng.*, **30**, 742 (2019), <https://doi.org/10.14478/ace.2019.1092>
- M. Shaban, F. A. Elwahab, A. E. Ghitas and M. Y. El Zayat, *J. Sol-Gel Sci. Technol.*, **95**, 276 (2020), <https://doi.org/10.1007/s10971-020-05331-x>
- S. P. Buthelezi, A. O. Olaniran and B. Pillay, *Molecules*, **17**, 14260 (2012), <https://doi.org/10.3390/molecules171214260>
- M. El Batouti, N. F. Alharby and M. M. Elewa, *Separations*, **9**, 1 (2021), <https://doi.org/10.3390/separations9010001>
- M. El Batouti, N. F. Al-Harby and M. M. Elewa, *Water*, **13**, 3241 (2021), <https://doi.org/10.3390/w13223241>
- Y. Ibrahim, V. Naddeo, F. Banat and S. W. Hasan, *Separ. Purif. Technol.*, **250**, 117250 (2020), <https://doi.org/10.1016/j.seppur.2020.117250>
- C. Zhang, K. T. Valsaraj, W. D. Constant and D. Roy, *Water Res.*, **33**, 115 (1999), [https://doi.org/10.1016/S0043-1354\(98\)00170-5](https://doi.org/10.1016/S0043-1354(98)00170-5)
- E. M. Cuerda-Correa, M. F. Alexandre-Franco C. and Fernández-González, *Water*, **12**, 102 (2019), <https://doi.org/10.3390/w12010102>
- Q. Chen, Z. Luo, C. Hills, G. Xue and M. Tyrer, *Water Res.*, **43**, 2605 (2009), <https://doi.org/10.1016/j.watres.2009.03.007>
- M. Vakili, M. Rafatullah, B. Salamatinia, A. Z. Abdullah, M. H. Ibrahim *et al.*, *Carbohydr. Polym.*, **113**, 115 (2014), <https://doi.org/10.1016/j.carbpol.2014.07.007>
- Z. Shariatnia and A. M. Jalali, *Int. J. Biol. Macromol.*, **115**, 194 (2018), <https://doi.org/10.1016/j.ijbiomac.2018.04.034>
- R. A. Alharbi, F. M. Alminderej, N. F. Al-harby, N. Y. Elmehbad and N. A. Mohamed, *Polymers*, **15**, 1529 (2023), <https://doi.org/10.3390/polym15061529>
- N. F. El-Harby, S. M. A. Ibrahim and N. A. Mohamed, *Water Sci. Technol.*, **76**, 2719 (2017), <https://doi.org/10.2166/wst.2017.442>
- J. Sh. Alnawmasi, *Carbohydr. Polym.*, **308**, 120596 (2023), <https://doi.org/10.1016/j.carbpol.2023.120596>
- N. F. Al-Harby, E. F. Albahly and N. A. Mohamed, *Polymers*, **14**, 271 (2022), <https://doi.org/10.3390/polym14020271>
- P. Sahariah and M. Másson, *Biomacromolecules*, **18**, 3846 (2017), <https://doi.org/10.1021/acs.biomac.7b01058>
- R. A. Alharbi, F. M. Alminderej, N. F. Al-harby, N. Y. Elmehbad and N. A. Mohamed, *Polymers*, **15**, 980 (2023), <https://doi.org/10.3390/polym15040980>
- N. F. Al-Harby, E. F. Albahly and N. A. Mohamed, *Polymers*, **13**, 4446 (2021), <https://doi.org/10.3390/polym13244446>
- D. C. Da Silva Alves, B. Healy, L. A. D. A. Pinto, T. R. S. A. Cadaval Jr. and C. B. Breslin, *Molecules*, **26**, 594 (2021), <https://doi.org/10.3390/molecules26030594>
- N. A. Mohamed and N. A. Abd El-Ghany, *Int. J. Polym. Mater. Polym. Biomater.*, **66**, 410 (2017), <https://doi.org/10.1080/00914037.2016.1233419>
- N. Y. Elmehbad, N. A. Mohamed and N. A. Abd El-Ghany, *Int. J. Biol. Macromol.*, **205**, 719 (2022), <https://doi.org/10.1016/j.ijbiomac.2022.03.076>
- M. W. Sabaa, N. A. Mohamed, R. R. Mohamed, N. M. Khalil and S. M. Abd El Latif, *Carbohydr. Polym.*, **79**, 998 (2010), <https://doi.org/10.1016/j.carbpol.2009.10.024>

- ²⁶ N. A. Mohamed and N. A. Abd El-Ghany, *J. Carbohyd. Chem.*, **31**, 220 (2012), <https://doi.org/10.1080/07328303.2011.650338>
- ²⁷ A. Abraham, P. A. Soloman and V. O. Rejini, *Proc. Technol.*, **24**, 741 (2016), <https://doi.org/10.1016/j.proctcy.2016.05.206>
- ²⁸ M. W. Sabaa, H. M. Abdallah, N. A. Mohamed and R. R. Mohamed, *Mater. Sci. Eng. C*, **56**, 363 (2015), <https://doi.org/10.1016/j.msec.2015.06.043>
- ²⁹ R. T. Alfuraydi, F. M. Alminderej and N. A. Mohamed, *Polymers*, **14**, 1619 (2022), <https://doi.org/10.3390/polym14081619>
- ³⁰ N. A. Mohamed and N. A. Abd El-Ghany, *Int. J. Biol. Macromol.*, **115**, 651 (2018), <https://doi.org/10.1016/j.ijbiomac.2018.04.101>
- ³¹ N. A. Mohamed, N. F. Al-Harby and M. S. Almarshed, *Int. J. Biol. Macromol.*, **132**, 416 (2019), <https://doi.org/10.1016/j.ijbiomac.2019.03.195>
- ³² N. Y. Elmehbad and N. A. Mohamed, *Int. J. Polym. Mater. Polym. Biomater.*, **71**, 969 (2022), <https://doi.org/10.1080/00914037.2021.1933975>
- ³³ N. A. Mohamed and N. Y. Al-mehbad, *Int. J. Biol. Macromol.*, **57**, 111 (2013), <https://doi.org/10.1016/j.ijbiomac.2013.03.007>
- ³⁴ N. A. Mohamed, N. A. Abd El-Ghany and M. M. Fahmy, *Int. J. Biol. Macromol.*, **82**, 589 (2016), <https://doi.org/10.1016/j.ijbiomac.2015.09.023>
- ³⁵ N. A. Mohamed, N. A. Abd El-Ghany and M. M. Abdel-Aziz, *Int. J. Biol. Macromol.*, **181**, 956 (2021), <https://doi.org/10.1016/j.ijbiomac.2021.04.095>
- ³⁶ N. A. Mohamed, A. El-Ghany and A. Nahed, *Cellulose*, **26**, 1141 (2019), <https://doi.org/10.1007/s10570-018-2096-5>
- ³⁷ N. Y. Elmehbad and N. A. Mohamed, *Int. J. Biol. Macromol.*, **151**, 92 (2020), <https://doi.org/10.1016/j.ijbiomac.2020.01.298>
- ³⁸ P. R. Chang, P. Zheng, B. Liu, D. P. Anderson, J. Yu *et al.*, *J. Hazard. Mater.*, **186**, 2144 (2011), <https://doi.org/10.1016/j.jhazmat.2010.12.119>
- ³⁹ B. Pan and B. Xing, *Environ. Sci. Technol.*, **42**, 9005 (2008), <https://doi.org/10.1021/es801777n>
- ⁴⁰ N. A. Mohamed, N. F. Al-Harby and M. S. Almarshed, *Polym. Bull.*, **77**, 6135 (2020), <https://doi.org/10.1007/s00289-019-03058-6>
- ⁴¹ N. A. Mohamed, N. F. Al-Harby and M. S. Almarshed, *Polym. Polym. Compos.*, **29**, S274 (2021), <https://doi.org/10.1177/0967391121999364>
- ⁴² K. Shukla, A. Verma, L. Verma, S. Rawat and J. Singh, *Nature Environ. Pollut. Technol.*, **19**, 57 (2020), [https://neptjournal.com/upload-images/\(5\)B-3615-ap.pdf](https://neptjournal.com/upload-images/(5)B-3615-ap.pdf)
- ⁴³ U. Yunusa, B. Usman and M. B. Ibrahim, *Int. J. Eng. Manuf.*, **10**, 54 (2020), <https://doi.org/10.5815/ijem.2020.04.05>
- ⁴⁴ M. H. Dehghani, A. Dehghan and A. Najafpoor, *J. Ind. Eng. Chem.*, **51**, 185 (2017), <https://doi.org/10.1016/j.jiec.2017.03.001>
- ⁴⁵ F. C. Wu, R. L. Tseng, S. C. Huang and R. S. Juang, *Chem. Eng. J.*, **151**, 1 (2009), <https://doi.org/10.1016/j.cej.2009.02.024>
- ⁴⁶ D. Kołodyńska, P. Hałas, M. Franus and Z. Hubicki, *J. Ind. Eng. Chem.*, **52**, 187 (2017), <https://doi.org/10.1016/j.jiec.2017.03.043>
- ⁴⁷ N. F. Alharby, R. S. Almutairi and N. A. Mohamed, *Polymers*, **13**, 3659 (2021), <https://doi.org/10.3390/polym13213659>
- ⁴⁸ J. Venkatesan, R. Jayakumar, A. Mohandas, I. Bhatnagar and S. K. Kim, *Materials*, **7**, 3946 (2014), <https://doi.org/10.3390/ma7053946>
- ⁴⁹ J. Zhang, Q. Zhou and L. Ou, *J. Chem. Eng. Data*, **57**, 412 (2012), <https://doi.org/10.1021/je2009945>
- ⁵⁰ A. Hamd, A. R. Dryaz, M. Shaban, H. AlMohamadi, K. A. Abu Al-Ola *et al.*, *Nanomaterials*, **11**, 2441 (2021), <https://doi.org/10.3390/nano11092441>
- ⁵¹ A. Rodríguez, G. Ovejero, J. L. Sotelo, M. Mestanza and J. Garcia, *J. Environ. Sci. Health Part A*, **45**, 1642 (2010), <https://doi.org/10.1080/10934529.2010.506137>
- ⁵² A. Dal Pozzo, L. Vanini, M. Fagnoni, M. Guerrini, A. De Benedittis *et al.*, *Carbohyd. Polym.*, **42**, 201 (2000), [https://doi.org/10.1016/S0144-8617\(99\)00134-4](https://doi.org/10.1016/S0144-8617(99)00134-4)
- ⁵³ R. A. Muzzarelli, *Carbohyd. Polym.*, **84**, 54 (2011), <https://doi.org/10.1016/j.carbpol.2010.12.025>
- ⁵⁴ R. A. Muzzarelli, M. Weckx, O. Filippini and F. Sigon, *Carbohyd. Polym.*, **11**, 293 (1989), [https://doi.org/10.1016/0144-8617\(89\)90004-0](https://doi.org/10.1016/0144-8617(89)90004-0)
- ⁵⁵ G. Crini and P. M. Badot, *Progress Polym. Sci.*, **33**, 399 (2008), <https://doi.org/10.1016/j.progpolymsci.2007.11.001>
- ⁵⁶ A. A. Inyinbor, F. A. Adekola and G. A. Olatunji, *Appl. Water Sci.*, **7**, 2297 (2017), <https://doi.org/10.1007/s13201-016-0405-4>
- ⁵⁷ L. Ai, C. Zhang, F. Liao, Y. Wang, M. Li, *et al.*, *J. Hazard. Mater.*, **198**, 282 (2011), <https://doi.org/10.1016/j.jhazmat.2011.10.041>
- ⁵⁸ T. J. Al-Musawi, N. Mengelizadeh, O. Al Rawi and D. Balarak, *J. Polym. Environ.*, **30**, 344 (2022), <https://doi.org/10.1007/s10924-021-02200-8>
- ⁵⁹ R. L. Tseng and F. C. Wu, *J. Hazard. Mater.*, **155**, 277 (2008), <https://doi.org/10.1016/j.jhazmat.2007.11.061>
- ⁶⁰ T. Liu, Y. Li, Q. Du, J. Sun, Y. Jiao *et al.*, *Colloid. Surfaces B: Biointerf.*, **90**, 197 (2012), <https://doi.org/10.1016/j.colsurfb.2011.10.019>
- ⁶¹ M. H. Dehghani, A. Dehghan, H. Alidadi, M. Dolatabadi, M. Mehrabpour *et al.*, *Korean J. Chem. Eng.*, **34**, 1699 (2017), <https://doi.org/10.1007/s11814-017-0077-2>
- ⁶² R. Shahryari-Ghoshekandi and H. Sadegh, *Jordan J. Chem.*, **9**, 267 (2014), <https://platform.almanhal.com/Files/2/86364>
- ⁶³ M. El Haddad, R. Mamouni, N. Saffaj and S. Lazar, *J. Assoc. Arab Univ. Basic Appl. Sci.*, **12**, 48 (2012), <https://doi.org/10.1016/j.jaubas.2012.04.003>